Elastic interactions between topological defects in chiral nematic shells

Alexandre Darmon, Olivier Dauchot, Teresa Lopez-Leon, and Michael Benzaquen*
EC2M, UMR No. 7083, CNRS, Gulliver, ESPCI Paris, PSL Research University 10 Rue Vauquelin, 75005 Paris, France
(Received 2 August 2016; revised manuscript received 11 October 2016; published 5 December 2016)

We present a self-consistent and robust theoretical model to investigate elastic interactions between topological defects in liquid crystal shells. Accounting for the nonconcentric nature of the shell in a simple manner, we are able to successfully and accurately explain and predict the positions of the defects, most relevant in the context of colloidal self-assembly. We calibrate and test our model on existing experimental data and extend it to all observed defects configurations in chiral nematic shells. We perform experiments to check further and confirm the validity of the present model. Moreover, we are able to obtain quantitative estimates of the energies of $+1$ or $+3/2$ disclination lines in cholesterics, whose intricate nature was only reported recently [A. Darmon, *et al.* Proc. Natl. Acad. Sci. USA **113**, 9469 (2016)].

DOI: 10.1103/PhysRevE.94.062701

Topological defects are a common feature of many forms of condensed matter [1,2]. They are notably encountered in solids, for which they provide very specific electrical and mechanical properties [3]. Topological defects are also crucial in other fields such as magnetism [4] or cosmology [5]. Although the underlying physics is in each case different, the mathematical framework is universal: The defects are defined as singularities in the order parameter field. One of the most common occurrences of topological defects in condensed matter is in liquid crystals [6–8], where they have been widely studied since Lehmann's first description of liquid crystalline mesophases [9].

One of the simplest ways to stabilize defects in liquid crystals is to induce topological constraints [10]. When a two-dimensional nematic phase is coated onto the surface of a sphere, frustrations in the orientational order necessarily stem from curvature and result in the presence of topological defects. In this context, an original idea, proposed by Nelson [11], was to use spherical nematic particles as mesoscopic atoms. The defects could, once functionalized, act as sticky patches able to induce directional bonds between particles. These anisotropic building blocks are then expected to reproduce crystalline structures at the mesoscale via self-assembly. Good control over the valence, i.e., the number of defects, and the bond directionality, i.e., the position of the defects, is thus crucial in this context. Since Nelson's seminal paper, many experimental studies focused on nematic shells have demonstrated the applicability of such concepts [12–15]. In addition, unexpected symmetries and valences have been recently reported in cholesteric shells [16,17], in which there is a spontaneous helical arrangement of the director field. Remarkably, it is possible to achieve good control over the equilibrium defect positions by tuning the shell thickness heterogeneity [13,16,18]. This feature could then be further exploited to produce shells with a variable bonding directionality. Although numerical studies have been able to capture this idea at the qualitative level [18–21], no theoretical model is yet able to predict the equilibrium defect positions quantitatively, despite the potential interest for applications.

In this paper we present a robust and self-consistent approach to compute and predict defect positions in eccentric cholesteric shells (see Fig. 1). Minimizing the free energy, which we write as surface energy terms multiplied by carefully chosen shell thicknesses, we derive the angular positions of the defects as a function of the shell geometry for all possible defect configurations. We first compare our model to available experimental data on the tetravalent configuration, which notably allows us to set the value of the adjustable parameter of our model, namely, the minimum shell thickness. We then successively address all other defect configurations together with experimental data. After performing self-consistency checks, we use our model to estimate the energies of recently reported nontrivial defect structures. [16,17,22].

On a sphere, a two-dimensional in-plane director field must fulfill the topological requirements of the Poincaré-Hopf theorem [23–25]. The latter can be written as $\sum_i m_i = +2$, where m_i is the charge or winding number, quantifying the amount of rotation of the director field around defect i. Hence, an overall charge of $+2$ needs to be distributed over one or several defects, whose winding numbers are integers or half-integers, consistent with the twofold symmetry of the nematic phase. Theoretical calculations have shown that the ground state of such a system is tetravalent, composed of four $+1/2$ defects located at the vertices of a regular tetrahedron [26]. Interestingly, this configuration has been experimentally found in nematic and cholesteric shells [12,17]. Besides, four additional configurations with the following defect charges have been recently reported in chiral nematic shells [17]: (i) two $+1$ defects, (ii) one $+1$ defect and two $+1/2$ defects, (iii) one $+3/2$ defect and one $+1/2$ defect, and (iv) one $+2$ defect. In the following, we investigate each of the above configurations in the stated order for reasons that will become clear later in this paper.

Thickness heterogeneities in the shell are due to a density mismatch between the inner phase and the liquid crystal phase [see Fig. 1(a)]. As suggested in Refs. [13,20], we here quantitatively argue that the equilibrium positions of the defects result from a balance of two forces: (i) an elastic repulsion that drives defects away from each other and (ii) an attractive thickness gradient arising from the nonconcentricity of the shells (see Fig. 1). As a result, topological defects tend

*Present address: Capital Fund Management, 23 Rue de l'Université, 75007 Paris, France.

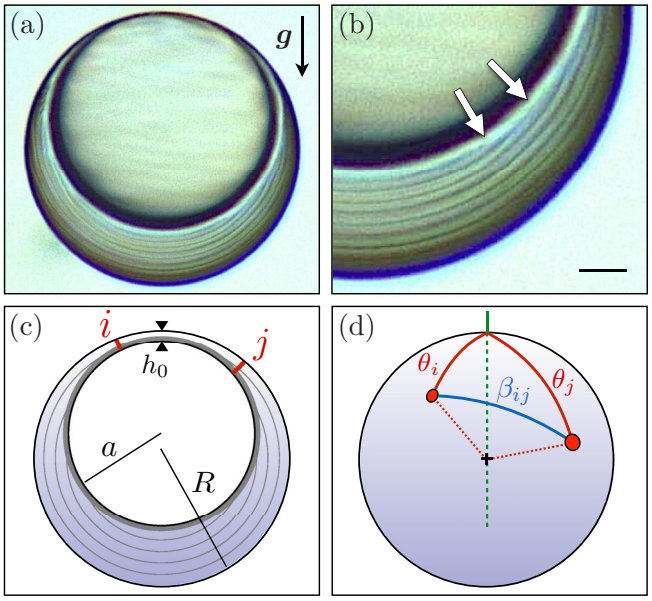

FIG. 1. (a) and (b) Side view optical microscopy pictures of an eccentric cholesteric liquid crystal shell. The scale bar is 10 μm. (c) Side view schematics of an eccentric shell. The concentric cholesteric layers are represented by thin solid gray lines. The thick gray line on the inner sphere signifies the region where the director field becomes slightly distorted to satisfy the tangential anchoring. (d) Schematics of defects on the outer sphere.

to regroup in the thinnest part of the shell. Figures 1(a) and 1(b) display a side imaging of a typical cholesteric shell. The uncompressed cholesteric layers are arranged as concentric spheres, starting from the outer surface of the shell, and the observed helical periodicity in the shell matches the actual pitch of the chiral solution, meaning that there is no frustration of the spontaneous cholesteric twist. Due to the presence of the inner droplet and the eccentric nature of the shell, each layer ends at a different position on the inner surface, as indicated by the arrows in Fig. 1(b). Note that this arrangement is, *a priori*, not compatible with a planar degenerate anchoring on the inner surface, suggesting the existence of a small region around the inner sphere where the director field becomes slightly distorted to overcome this issue [see Figs. 1(b) and 1(c)]. However, this surface contribution is *a priori* small compared to the other elastic costs in the system.

In cholesteric shells, the arrangement of the director field can thus be described as concentric layers with a helical twist matching the actual pitch of the cholesteric solution. Remarkably, if such a director field is introduced in the Frank-Oseen free-energy density, the twist term vanishes [27]. Theoretically, it was even shown that for cholesteric droplets, this director field minimizes the free energy of the system [27]. It is precisely the spontaneous cholesteric twist that makes the twist contribution null in these spherical systems. At the first level of approximation, we can thus ignore the details of the molecular ordering. In particular, since the spontaneous helical pitch is everywhere satisfied in this geometry, we consider the global cholesteric arrangement as a superposition of two-dimensional nematic layers. Interestingly, the above-mentioned onionlike arrangement ensured by the spontaneous twist is not necessarily present in nematic shells where the director field can have a non-negligible radial component [20,28]. For this reason, cholesteric shells are more adapted to our approach than their nematic counterparts.

In the one elastic constant approximation, the surface free energy E of a two-dimensional in-plane director field with topological defects interacting on a sphere can be written as [11]

$$E = \pi K \left(\sum_i E_i^0 + \sum_{i<j} U_{ij} \right), \tag{1}$$

where K is the elastic constant, E_i^0 the dimensionless energy of defect i, and U_{ij} the dimensionless interaction energy between defects i and j, with

$$E_i^0 = m_i^2 \log(R/r_{c,i}), \tag{2a}$$

$$U_{ij} = -m_i m_j \log(1 - \cos\beta_{ij}), \tag{2b}$$

where R is the sphere radius, $r_{c,i}$ the defect core radius, and β_{ij} the central angle between defects i and j [see Fig. 1(d)]. For small angles, Eq. (2b) reduces to

$$U_{ij} = -2m_i m_j \log(\beta_{ij}/\sqrt{2}). \tag{3}$$

In order to compute the total free energy of the system and account for the eccentric nature of the shell, we proceed as follows. Rather than performing a highly nontrivial integration of the energy over the nonconcentric system, we aim at capturing the essence of the interaction in a simple effective way. To do so, we multiply the different terms in the two-dimensional free energy of Eq. (1) by local shell thicknesses taken according to the physical grounds provided below. In the following, these thicknesses are expressed in units of the outer radius of the shell R. For the self-energy E_i^0, we simply use the local thickness of the shell at defect i, denoted h_i. For the interaction energy, we use the minimal thickness along the geodesic path between defects i and j on the outer sphere, denoted $h_{ij}^{\min}$. The reason is as follows. As mentioned above, the inner water droplet does not compress the cholesteric layers, which, on the contrary, are interrupted at its boundary [see Figs. 1(a) and 1(b)]. We thus assume that the defect interaction is mostly mediated by the elastic energy associated to the layers that are not disrupted by the inner droplet, the extension of those layers being proportional to $h_{ij}^{\min}$. The total dimensionless free energy $F = E/\pi K R$ of the eccentric liquid crystal shell can then be written as

$$F = \sum_i E_i^0 h_i + \sum_{i<j} U_{ij} h_{ij}^{\min}. \tag{4}$$

Multiplying by local thicknesses is at the core of the present model and corresponds to the simplest approach where the attractive thickness gradient is taken into account. The approach is thus expected to be most accurate when the defects are close to each other.

Due to the azimuthal symmetry of the eccentric shell, the local thickness of the shell denoted by h is a function of the polar angle θ only [see Fig. 1(d)]. As a result, the thicknesses involved in Eq. (4) are such that $h_i = h(\theta_i)$, where θ_i denotes the polar angle of defect i, and $h_{ij}^{\min} = h(\theta_{ij}^{\min})$, where $\theta_{ij}^{\min}$ is the polar angle where h is minimal along the geodesic path

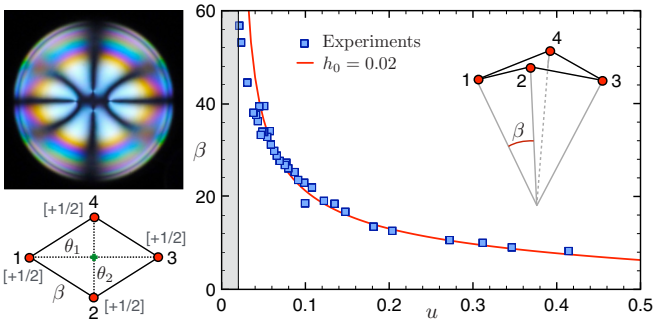

FIG. 2. Configuration with four +1/2 defects. Shown on the top left is the top view image between crossed polarizers of a 4[+1/2] nematic shell. The bottom left shows the schematics of the defect arrangement. On the right is the angular distance β between nearby defects as a function of u. The blue squares correspond to experimental data from [13] and the solid red line is the result of the minimization of the free energy in Eq. (7) with $h_0 = 0.02$.

between i and j. When varying the geometry of the shell, $h(\theta)$ is also an implicit function of two additional dimensionless parameters: (i) the renormalized minimal thickness h_0 and (ii) $u \equiv (R-a)/R$, where a denotes the inner radius of the shell [see Fig. 1(c)]. In our experiments, we observe that h_0 is constant and independent of the shell nature and geometry. On physical grounds, this can be explained by the fact that it is the disjoining pressure between the inner and outer interfaces that sets the value of h_0 [16] (see [18] for a recent numerical study on the effects of varying h_0). Hence, we are only left with the parameter u, which actually measures the thickness gradient within the shell, and thus rigorously write $h(\theta;u)$ for the local thickness. Finally, for each of the defect configurations, we minimize the total free energy F [see Eq. (4)] with respect to the angular positions and obtain the equilibrium angles as a function of u only. In the small-angle approximation, one can easily show using purely geometrical considerations that the local thickness $h(\theta;u)$ reads

$$h(\theta;u) = h_0 + g(u)\frac{\theta^2}{2} + o(\theta^2), \tag{5}$$

where g is a dimensionless function of u only, reading

$$g(u) = \frac{(1-h_0)(u-h_0)}{1-u}. \tag{6}$$

Let us start with the tetravalent 4[+1/2] configuration. To confront our model, we use experimental data of nematic shells from Ref. [13]. The reasons for such a choice are twofold. First, all defects in this configuration are singular lines such that the arrangement of the director field remains essentially two dimensional. As mentioned above, this feature is crucial in our approach. Second, the exact structure of those lines is well known, which, as we will see below, is not always the case in cholesterics. This configuration is thus the best candidate to check the validity of the present model. It is notably characterized by four outer defects located at the vertices of a folded rhombus (see Fig. 2). The experimental central angle β between two nearby defects, identical for each pair of defects and taken from Ref. [13], is plotted as a function of u. Noting that $\theta_1 = \theta_3$, $\theta_2 = \theta_4$, and $h(\theta_{13}^{\min};u) = h(\theta_{24}^{\min};u) = h_0$, the free energy of the 4[+1/2] configuration reads

$$F_{4[+1/2]}(\theta_1,\theta_2;u) = 4U_{12}h\left(\theta_{12}^{\min};u\right) + (U_{13}+U_{24})h_0 + 2E_1^0[h(\theta_1;u) + h(\theta_2;u)], \tag{7}$$

where the interaction energies read

$$U_{12}(\theta_1,\theta_2) = -\frac{1}{4}\log\left(\frac{\theta_1^2+\theta_2^2}{2}\right), \tag{8a}$$

$$U_{13}(\theta_1) = -\frac{1}{2}\log(\theta_1\sqrt{2}), \tag{8b}$$

$$U_{24}(\theta_2) = -\frac{1}{2}\log(\theta_2\sqrt{2}), \tag{8c}$$

and the angle $\theta_{12}^{\min}$ in Eq. (7) is given by

$$\theta_{12}^{\min} = \frac{\theta_1\theta_2}{\sqrt{\theta_1^2+\theta_2^2}}. \tag{9}$$

The two parameters θ_1 and θ_2 fully characterize the positions of the defects. We set $r_{c,1/2} \sim 10$ nm $\sim 10^{-4}R$ for $R = 100$ μm, consistently with reported values [8,29]. Minimizing the free energy with respect to θ_1 and θ_2 and noting that $\beta = \sqrt{\theta_1^2+\theta_2^2}$, we obtain the equilibrium curve $\beta(u)$ (see Fig. 2). Fitting the experimental data to $\beta(u)$ with respect to h_0 yields excellent agreement for $h_0 = 0.02$. The latter value of h_0, equal to 1 μm when $R = 50$ μm, is consistent with the current and previous experimental studies [13,16]. This first result can be seen as a calibration of the model and we will use the above value of h_0 as a reference throughout the following.

We now look into the configuration consisting of two +1 disclination lines. In Fig. 3 we report data obtained from a previous study [16], measured for shells with different cholesteric pitches $p = 9.3$, 6, and 3.6 μm (see green squares in Fig. 3). Noting that $\theta_1 = \theta_2 \equiv \theta$ and $h(\theta_{12}^{\min};u) = h_0$, the free energy of the 2[+1] configuration reads

$$F_{2[+1]}(\theta;u) = U_{12}h_0 + 2E_1^0 h(\theta;u), \tag{10}$$

where the interaction energy reads

$$U_{12}(\theta) = -2\log(\theta\sqrt{2}). \tag{11}$$

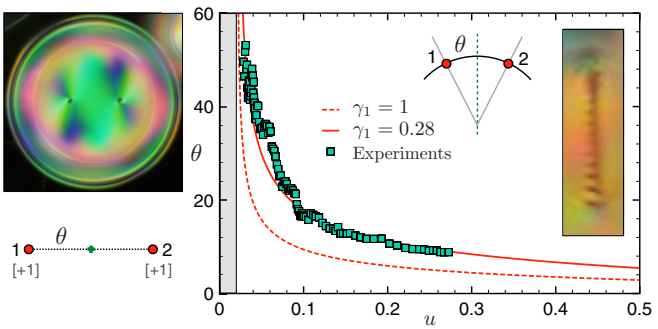

FIG. 3. Configuration with two +1 defects. Shown on the top left is the top view image between crossed polarizers of a 2[+1] cholesteric shell. The bottom left shows the schematics of defect arrangement. On the right is the angular position θ as a function of u. Green squares show the experimental data from [16] for which a rolling average was performed. The inset displays a picture of the intricate structure of the +1 disclination in a cholesteric shell.

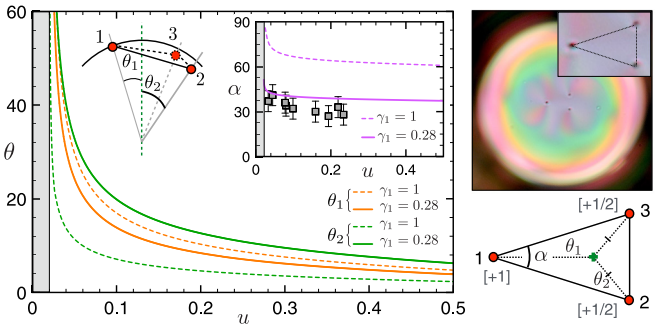

FIG. 4. Configuration with one +1 and two +1/2 defects. Shown on the left are angular positions θ_i as a function of u. The inset displays the vertex angle α of the isosceles triangle as a function of u (experimental results are shown as gray squares). The top right is top view image between crossed polarizers of a $[+1]+2[+1/2]$ cholesteric shell with a zoom-in on the defects (inset). The bottom right shows the schematics of the defect arrangement.

For this configuration as well as for the following, the core radii are set according to the reference value $r_{c,1/2}$ through $r_{c,i} = (m_i/m_j)r_{c,j}$ [29]. Minimization with respect to θ yields the red dashed line in Fig. 3, which does not quantitatively capture the experimental behavior. The reason is that +1 lines in cholesteric shells are actually not simple singular lines. Our recent experiments and numerical simulations [16] have shown that this structure is actually composed of a stack of disclination rings (see the inset of Fig. 3), with a director field escaping between each ring. The energy of such a defect is thus expected to be different from that of a purely singular line. The proper self-energy will then be written as $\gamma_1 E_1^0$, where γ_1 is a scalar that is *a priori* unknown. It is worth emphasizing here that only the self-energy of the defect is altered. Indeed, although the structure of the defect is intricate, it can still be seen as a +1 disclination when looking sufficiently far off. Hence, since the interaction energy is far field, it should not be affected by the details of the defect structure. The best fit is obtained for $\gamma_1 = 0.28$, displayed as a solid red line in Fig. 3. Note that we obtain $\gamma_1 < 1$, which is fully consistent with the escaped nature of the disclination. It is worth mentioning that this approach, which we will self-consistently validate below, actually represents a method to experimentally estimate the energy of this intricate structure.

Having addressed configurations made of +1/2 and +1 defects only, the next logical step consists in studying a configuration containing both, namely, the triangular configuration $[+1]+2[+1/2]$. To fully parametrize the positions of the defects on the outer sphere, three independent parameters, namely, $\theta_1, \theta_2(=\theta_3)$, and α, which is the vertex angle of the isosceles triangle, must be considered (see Fig. 4). The dimensionless free energy can be written as

$$F_{\text{triangle}}(\theta_1,\theta_2,\alpha;u) = 2U_{12}h\left(\theta_{12}^{\min};u\right) + U_{23}h\left(\theta_{23}^{\min};u\right) + \gamma_1 E_1^0 h(\theta_1;u) + 2E_2^0 h(\theta_2;u), \quad (12)$$

where the interaction energies in Eq. (12) read

$$U_{12}(\theta_1,\theta_2,\alpha) = -\log\left(\frac{\beta_{12}}{\sqrt{2}}\right), \quad (13)$$

$$U_{13}(\theta_1,\theta_2,\alpha) = -\frac{1}{2}\log\left(\frac{\beta_{23}}{\sqrt{2}}\right), \quad (14)$$

with central angles reading

$$\beta_{12} = \theta_1\cos\left(\frac{\alpha}{2}\right) + \sqrt{\theta_2^2 - \theta_1^2\sin^2\left(\frac{\alpha}{2}\right)}, \quad (15)$$

$$\beta_{23} = 2\sin\left(\frac{\alpha}{2}\right)\left[\theta_1\cos\left(\frac{\alpha}{2}\right) + \sqrt{\theta_2^2 - \theta_1^2\sin^2\left(\frac{\alpha}{2}\right)}\right], \quad (16)$$

and the angles $\theta_{12}^{\min}$ and $\theta_{32}^{\min}$ in Eq. (12) reading

$$\theta_{12}^{\min} = \cos\left(\frac{\alpha}{2}\right)\left[\theta_1\cos\left(\frac{\alpha}{2}\right) + \sqrt{\theta_2^2 - \theta_1^2\sin^2\left(\frac{\alpha}{2}\right)}\right] - \theta_1, \quad (17)$$

$$\theta_{23}^{\min} = \frac{1}{2}\tan\left(\frac{\alpha}{2}\right)\left[\theta_1\cos\left(\frac{\alpha}{2}\right) + \sqrt{\theta_2^2 - \theta_1^2\sin^2\left(\frac{\alpha}{2}\right)}\right]. \quad (18)$$

We note that the self-energy of the +1 defect has naturally been set to $\gamma_1 E_1^0$, consistent with the $2[+1]$ case, and E_2^0 denotes the self-energy of the +1/2 defects. The equilibrium solutions θ_1 and θ_2 are displayed in Fig. 4, for both $\gamma_1 = 1$ (dashed lines) and $\gamma_1 = 0.28$ (solid lines). Most importantly, when plotting the vertex angle α as a function of u (see the inset of Fig. 4), we see that this angle is actually much larger for $\gamma_1 = 1$ than for $\gamma_1 = 0.28$. To compare this theoretical prediction of the vertex angle to experimental data, we have generated cholesteric shells using microfluidics [12,30] and measured α for different cholesteric shells (see the gray squares in the inset of Fig. 4). One can see that the model with $\gamma_1 = 0.28$ is clearly better than with $\gamma_1 = 1$. The results on the triangle configuration constitute a self-consistency check that validates the model and confirms the estimate of the energy found for the intricate +1 disclination in cholesteric shells.

Let us finally investigate the last configuration, composed of two defects of nonequal charges +3/2 and +1/2 [17]. In the following, the indices 1 and 2, respectively, correspond to the +3/2 and +1/2 defects (see Fig. 5). In this configuration, the dimensionless free energy reads

$$F_{[+3/2]+[+1/2]}(\theta_1,\theta_2;u) = U_{12}h_0 + E_1^0 h(\theta_1;u) + E_2^0 h(\theta_2;u), \quad (19)$$

where the interaction energy reads

$$U_{12}(\theta_1,\theta_2) = -\frac{3}{2}\log\left(\frac{\theta_1+\theta_2}{\sqrt{2}}\right). \quad (20)$$

The equilibrium angles θ_1 and θ_2 are plotted as a function of u in Fig. 5 (dashed lines). As expected, since E_1^0 is much larger than E_2^0, θ_1 is much smaller than θ_2 for all u. However, our experiments reveal that $\theta_{1,\text{expt}} \simeq \theta_{2,\text{expt}}$ for all u, meaning that the true energy of the +3/2 line should be very much comparable to that of the +1/2. Hence, the energy of the +3/2 disclination must be corrected by a factor denoted by $\gamma_{3/2}$. This necessary correction is, here as well, consistent with the

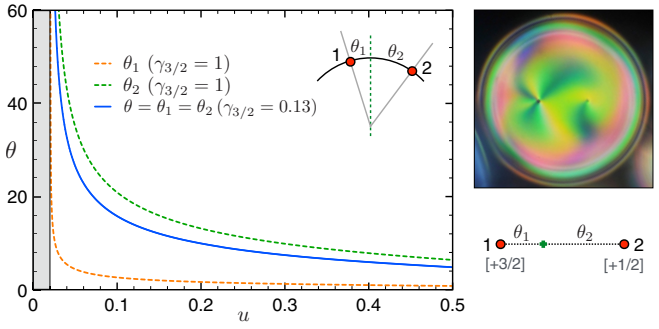

FIG. 5. Configuration with one $+3/2$ defect and one $+1/2$ defect. Shown on the left are angular positions θ_i as a function of u. The top right is the top view image between crossed polarizers of a $[+3/2]+[+1/2]$ cholesteric shell. The bottom right shows the schematics of the defect arrangement.

intricate structure of the nonregular $+3/2$ defect line, actually made of a nonsingular disclination wound around another singular line [17]. To match the experimental observations, the energy of the real $+3/2$ line must naturally be equal to that of the $+1/2$ line; one finds $\gamma_{3/2} = E_2^0/E_1^0 \simeq 0.13$ (see the solid blue line in Fig. 5). Finally, the single $+2$ defect equilibrium configuration is trivial, as there is no interaction term U_{ij}; it is naturally always located at $\theta = 0$.

We have shown that our self-consistent model is able to successfully explain and predict defect positions in chiral nematic shells. In the context of colloidal self-assembly, fine-tuning of defect positions is of crucial importance as it controls the bond directionality of these superatom candidates [11,13]. Moreover and equally important, our model allows us to estimate the energies of the recently reported highly nontrivial structures displayed by cholesterics in spherical geometries. More generally, the framework developed in this paper opens the way to a method to measure unknown energies of defect cores.

We thank A. Fernandez-Nieves for fruitful discussions. We acknowledge support from Institut Pierre-Gilles de Gennes (Laboratoire d'Excellence, Investissements d'Avenir Programs No. ANR-10-IDEX 0001-02 PSL and No. ANR-10-EQPX-31) as well as the French National Research Agency (ANR) through Grant No. 13-JS08-0006-01.

[1] N. D. Mermin, Rev. Mod. Phys. **51**, 591 (1979).
[2] D. R. Nelson, *Defects and Geometry in Condensed Matter Physics* (Cambridge University Press, Cambridge, 2002).
[3] T. Mura, *Micromechanics of Defects in Solids* (Springer Science and Business Media, New York, 2013).
[4] X. Z. Yu, Y. Onose, N. Kanazawa, J. H. Park, J. H. Han, Y. Matsui, N. Nagaosa, and Y. Tokura, Nature (London) **465**, 901 (2010).
[5] T. W. B. Kibble, in *Topological Defects and the Non-Equilibrium Dynamics of Symmetry Breaking Phase Transitions*, edited by Y. M. Bunkov and H. Godfrin, NATO Science Series, Series C: Mathematical and Physical Sciences (Springer Netherlands, Dordrecht, 2000), Vol. 549.
[6] K. Jänich, Acta Appl. Math **8**, 65 (1987).
[7] M. Kléman, Rep. Prog. Phys. **52**, 555 (1989).
[8] P.-G. de Gennes and J. Prost, *The Physics of Liquid Crystals*, 2nd ed. (Oxford University Press, New York, 1993).
[9] O. Lehmann, *Flüssige Kristalle* (Engelmann, Leipzig, 1904).
[10] O. D. Lavrentovich, Liq. Cryst. **24**, 117 (1998).
[11] D. R. Nelson, Nano Lett. **2**, 1125 (2002).
[12] A. Fernández-Nieves, V. Vitelli, A. S. Utada, D. R. Link, M. Márquez, D. R. Nelson, and D. A. Weitz, Phys. Rev. Lett. **99**, 157801 (2007).
[13] T. Lopez-Leon, V. Koning, K. B. S. Devaiah, V. Vitelli, and A. Fernandez-Nieves, Nat. Phys. **7**, 391 (2011).
[14] T. Lopez-Leon, M. A. Bates, and A. Fernandez-Nieves, Phys. Rev. E **86**, 030702 (2012).
[15] M. A. Gharbi, D. Seč, T. Lopez-Leon, M. Nobili, M. Ravnik, S. Žumer, and C. Blanc, Soft Matter **9**, 6911 (2013).
[16] A. Darmon, M. Benzaquen, D. Seč, S. Čopar, O. Dauchot, and T. Lopez-Leon, Proc. Natl. Acad. Sci. USA **113**, 9469 (2016).
[17] A. Darmon, M. Benzaquen, S. Čopar, O. Dauchot, and T. Lopez-Leon, Soft Matter **12**, 9280 (2016).
[18] Y. Zhou, A. Guo, R. Zhang, J. C. Armas-Perez, J. A. Martínez-González, M. Rahimi, M. Sadati, and J. J. de Pablo, Soft Matter **12**, 8983 (2016).
[19] D. Seč, T. Lopez-Leon, M. Nobili, C. Blanc, A. Fernandez-Nieves, M. Ravnik, and S. Žumer, Phys. Rev. E **86**, 020705 (2012).
[20] V. Koning, T. Lopez-Leon, A. Fernandez-Nieves, and V. Vitelli, Soft Matter **9**, 4993 (2013).
[21] C. R. Wand and M. A. Bates, Phys. Rev. E **91**, 012502 (2015).
[22] D. Seč, T. Porenta, M. Ravnik, and S. Žumer, Soft Matter **8**, 11982 (2012).
[23] H. Poincaré, J. Math. Pure Appl. **1**, 167 (1885).
[24] H. Hopf, Math. Ann. **96**, 427 (1926).
[25] R. D. Kamien, Rev. Mod. Phys. **74**, 953 (2002).
[26] T. Lubensky and J. Prost, J. Phys (France) II **2**, 371 (1992).
[27] J. Bezić and S. Žumer, Liq. Cryst. **11**, 593 (1992).
[28] V. Vitelli and D. R. Nelson, Phys. Rev. E **74**, 021711 (2006).
[29] P. Oswald and P. Pieranski, *Nematic and Cholesteric Liquid Crystals* (Taylor & Francis, London, 2005).
[30] A. S. Utada *et al.*, Science **308**, 537 (2005).